# Model Based Inertial Sensing for Measuring the Kinematics of Sit-to-Stand Motion

JOSIP MUSIĆ*, ROMAN KAMNIK**, VLASTA ZANCHI*, MARKO MUNIH**
*Faculty of Electrical Engineering, Mechanical Engineering and Naval Architecture
University of Split
Ruđera Boškovića bb, 21000 Split
CROATIA
**Faculty of Electrical Engineering
University of Ljubljana
Tržaška 25, 1000 Ljubljana
SLOVENIA

*Abstract:* - In this paper a method for measuring kinematics of sit-to-stand movement using inertial sensors and human body model is presented. The proposed approach fuses data from inertial sensors (accelerometers and gyroscopes) and data from three-segment human body model using Extended Kalman filtering technique and in this way reduces inaccuracies associated with inertial sensors. Dynamic human body model is constructed based on principles of Lagrangian dynamics and incorporates shank, thigh and HAT (Head-Arms-Trunk) segments. The model equations, which are non-linear and coupled differential equations, are incorporated in the EKF to produce better kinematic parameter estimation of sit-to-stand motion. The moments needed in model equations (ankle, knee and hip moments) are calculated based on EKF last best estimate and Newton-Euler inverse dynamic approach. Outputs from EKF are segmental angles, angular rates of change and angular accelerations. These parameters fully describe the motion kinematics of human body. The performance of the method is verified by reference measurements acquired with optical motion measurement system Optotrak. Obtained results are presented and discussed. Conclusions are drawn and guidelines for future method improvement are suggested.

*Key-Words:* - **inertial sensors, human dynamic body model, extended kalman filter, sit-to-stand transfer**

## 1 Introduction

Microelectromechanical (MEMS) inertial sensors have become widely available over the last few years [1]. Their small size and low cost have made them attractive for wide range of applications in different research areas: robotics, navigation and attitude-control systems, man-machine interface, virtual reality [2], analysis of human motion [3, 4] etc.

When performing dynamic analysis of human motion, the knowledge of translational and angular velocities and accelerations of segmental centers of masses (CoM) is of importance [5]. To measure these kinematic parameters body mounted inertial sensors attached to the human body segment of interest, can be used. These sensors have significant advantages over more sophisticated motion analysis systems commonly used today like Optotrak – Northern Digital Inc. or Vicon - Vicon Motion Systems: a) they are lightweight and portable, b) they don't require complicated and time consuming setting up procedures, c) they are unobtrusive since they don't constrain user in motion, d) and they are less expensive.

Despite their advantages inertial sensors also have their share of drawbacks [5, 6]. The dynamic and gravitational component in accelerometer output signal can't easily be distinguished during faster movements and the drift in gyroscope output signal results in large integration errors. These errors can be reduced by introduction of the magnetometer to the sensor pack and application of Kalman filtering technique to fuse the outputs from all the sensors [2, 7]. This method yields good results but introduces some additional restrictions on measurement setup, which can not easily be fulfilled in average ambulatory setting. Special care has to be given to avoid large metal or magnetic objects in the sensor vicinity because such objects can potentially become noise sources for magnetometer [7].

In our proposal we assume that magnetometer can be substituted in certain applications, by introduction of equations of dynamic human body model. In this approach, named model based inertial

sensing [8], data acquired from inertial sensors and data from dynamic human body model [9] are fused using Extended Kalman Filter (EKF) [10].

The paper presents the development of model based inertial sensing of human body kinematics in sit-to-stand motion and is structured as follows. In Section 2 construction of dynamic human body model is presented. Next, the accelerometer signal decomposition is explained and EKF designed outlined. In Section 3 obtained results are presented followed by explanation of some phenomena's in the results. Finally in Section 4 conclusions are drawn and guidelines for future method improvement are suggested.

# 2 Materials and methods

## 2.1 Dynamic human body model

The proposed method is based on dynamic three-segment human body model. The model consists of three rigid bodies corresponding to shank, thigh and HAT (head-arms-trunk) segments (see Figure 1).

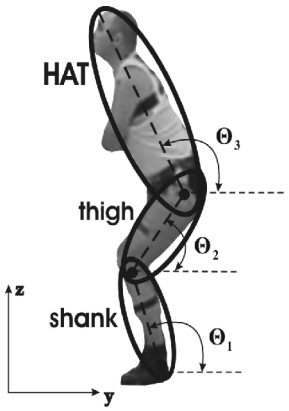


Fig. 1 – Three segment human body model

In figure $\Theta_i$ (i=1, 2, 3) represents segmental angles with respect to horizontal *y* axis.

During the modeling phase the following simplifications were introduced into the model: a) body motion is constrained to a sagittal plane, b) symmetry of sit-to-stand motion is assumed, c) joints are assumed to be ideal with no friction during rotation, d) each segment is assumed to be rigid with its mass contained at CoM. Model equations describing motion of each segment are derived using principles of Lagrangian dynamics. For each degree of freedom the Lagrangian equation is written:

$$\frac{d}{dt}\left(\frac{\partial K}{\partial \dot{\Theta}_i}\right) - \frac{\partial K}{\partial \Theta_i} + \frac{\partial V}{\partial \Theta_i} = T_i \qquad (1)$$

where:

K – is kinetic energy of *i*-th segment,
V – is potential energy of *i*-th segment, and
T – is generalized forces/moments acting on *i*-th segment .

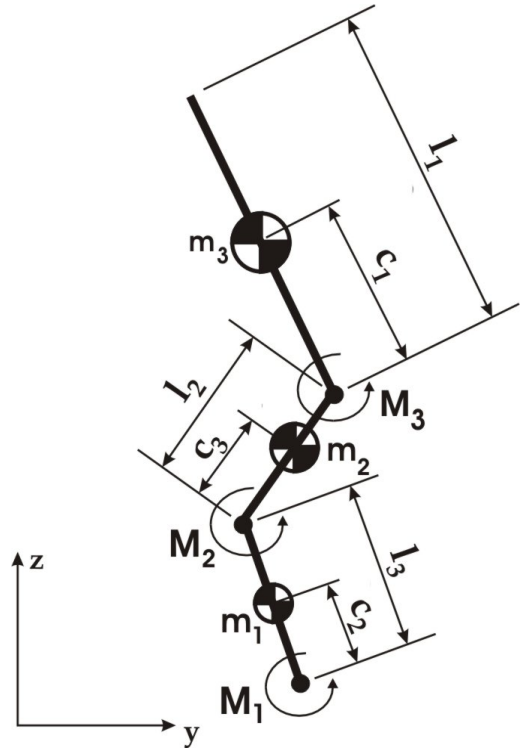


Fig. 2 – Three segment human model geometry and notation of parameters

Figure 2 depicts geometry of a model and notation used in modeling phase. The notation is

$M_1, M_2, M_3$ - ankle, knee and hip moments,
$m_i$ - mass of the *i*-th segment,
$l_i$ - length of the *i*-th segment,
$c_i$ - distance of segmental center of mass (CoM) from distal joint.

Anthropometric data i.e. segmental masses, lengths and CoM location are obtained from the literature [11]. Using (1) and notation from Figure 2, equations of motion for shank (2), thigh (3) and HAT (4) segments are derived. These equations are non-linear and coupled differential equations. From (2)-(4) segmental angles, angular velocities and angular accelerations can be calculated which fully describe the motion kinematics of human body.

$$\ddot{\Theta}_1(m_1c_1^2+m_2l_1^2+m_3l_1^2+I_{x1})+\ddot{\Theta}_2\cos(\Theta_1-\Theta_2)(m_2l_1c_2+m_3l_1l_2)+\ddot{\Theta}_3\cos(\Theta_1-\Theta_3)m_3l_1c_3+$$
$$\dot{\Theta}_2^2\sin(\Theta_1-\Theta_2)(m_2l_1c_2+m_3l_1l_2)+\dot{\Theta}_3^2\sin(\Theta_1-\Theta_3)m_3l_1c_3+g(m_1c_1+m_2l_1+m_3l_1)\cos\Theta_1=M_1-M_2 \quad (2)$$

$$\ddot{\Theta}_2(m_2c_2^2+m_3l_2^2+I_{x2})+\ddot{\Theta}_1\cos(\Theta_1-\Theta_2)(m_2l_1c_2+m_3l_1l_2)+\ddot{\Theta}_3\cos(\Theta_2-\Theta_3)m_3l_2c_3-$$
$$\dot{\Theta}_1^2\sin(\Theta_1-\Theta_2)(m_2l_1c_2+m_3l_1l_2)+\dot{\Theta}_3^2\sin(\Theta_2-\Theta_3)m_3l_2c_3+g(m_2c_2+m_3l_2)\cos\Theta_2=M_2-M_3 \quad (3)$$

$$\ddot{\Theta}_3(m_3c_3^2+I_{x3})+\ddot{\Theta}_1\cos(\Theta_1-\Theta_3)m_3l_1c_3+\ddot{\Theta}_2\cos(\Theta_2-\Theta_3)m_3l_2c_3-$$
$$\dot{\Theta}_1^2\sin(\Theta_1-\Theta_3)m_3l_1c_3-\dot{\Theta}_2^2\sin(\Theta_2-\Theta_3)m_3l_2c_3+gm_3c_3\cos\Theta_3=M_3 \quad (4)$$

## 2.2 Accelerometer signal decomposition

Inertial accelerometer output signal consists of two main components, the dynamic and gravitational. These components can only be distinguished when motion of accelerometer is quasi-static [3]. The problems arise when the motion is not aligned with accelerometer sensitive axis, in which case the true acceleration is projected onto accelerometer sensitive axis along with gravitational component. Sum of two components represents the accelerometer output for the sensitive axis. Since the accelerations expressed in certain reference frame are of interest, processing of the accelerometer output signal is needed. In order to obtain accelerations along $z_{REF}$ and $y_{REF}$, the decomposition of the accelerometer signal to its main components, and back projection onto the reference frame is required. For this the angle between sensor's and reference frames needs to be known.

The sensor angle is defined as the angle between the *z* axis of the sensor and the *y* reference axis as shown in Figure 3. This angle was chosen as it is in accordance with equations of dynamic human body model. The component that is of interest is acceleration projection component which is then projected back onto $z_{REF}$ axis yielding sensor true acceleration in $z_{REF}$ direction. Because of the nature of inertial sensing, the dynamic acceleration output is opposite to true direction of motion. The accelerometer signal decomposition for *z* component is graphically depicted in Figure 3 and is defined by

$$a_{z_{SENSOR}} = -(a_{z_{REF}}\sin\Theta + g\sin\Theta) \quad (5)$$

for *z* component, and

$$a_{y_{SENSOR}} = a_{y_{REF}}\sin\Theta - g\cos\Theta \quad (6)$$

for *y* component.

The sensor angle $\Theta$ in (5) and (6) is available as system state of the EKF.

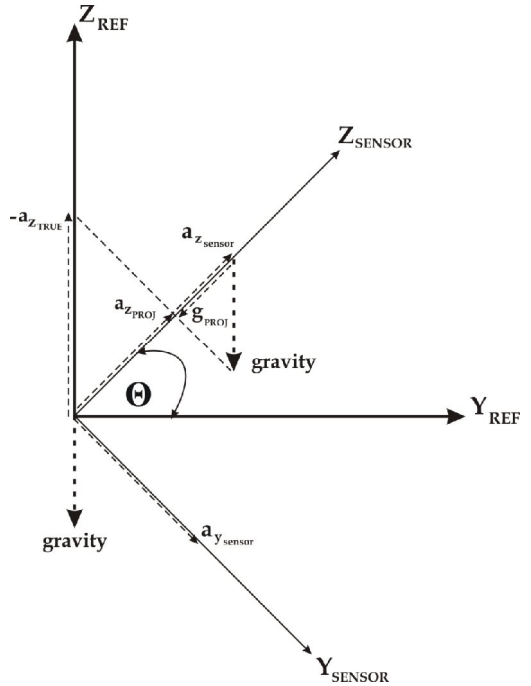


Fig. 3 – Accelerometer signal decomposition

## 2.3 Extended Kalman Filter architecture

In the proposed method the Extended Kalman Filter (EKF) is employed for fusion of the acquired accelerometry data and data from dynamic human body model. In EKF the system is described by:
the system equation

$$\dot{\mathbf{x}} = \mathbf{A}\cdot\mathbf{x} + \mathbf{w} \quad (6)$$

and the measurement equation

$$\mathbf{z} = \mathbf{h}(\mathbf{x}, \mathbf{v}) \quad (7)$$

In (6) **x** describes the state vector and **w** the white process noise, while in (7) **h** is measurement vector and **v** is the white measurement noise. It is assumed that noises **v** and **w** are Gaussian distributed, have zero mean and are uncorrelated.

During the EKF design process, several architectures were tested. The selected structure (8), (9) demonstrated best performance.

$$\begin{bmatrix} h_1 \\ h_2 \\ h_3 \\ h_4 \\ h_5 \\ h_6 \\ h_7 \\ h_8 \\ h_9 \\ h_{10} \\ h_{11} \\ h_{12} \end{bmatrix} = \begin{bmatrix} \dot{\Theta}_1 \\ \dot{\Theta}_2 \\ \dot{\Theta}_3 \\ (-c_1\ddot{\Theta}_1 \sin\Theta_1 - c_1\dot{\Theta}_1^2 \cos\Theta_1)\sin\Theta_1 - g\cos\Theta_1 \\ -(c_1\ddot{\Theta}_1 \cos\Theta_1 - c_1\dot{\Theta}_1^2 \sin\Theta_1)\sin\Theta_1 - g\sin\Theta_1 \\ (-l_1\ddot{\Theta}_1 \sin\Theta_1 - l_1\dot{\Theta}_1^2 \cos\Theta_1 - c_2\ddot{\Theta}_2 \sin\Theta_2 - c_2\dot{\Theta}_2^2 \cos\Theta_2)\sin\Theta_2 - g\cos\Theta_2 \\ -(l_1\ddot{\Theta}_1 \cos\Theta_1 - l_1\dot{\Theta}_1^2 \sin\Theta_1 + c_2\ddot{\Theta}_2 \cos\Theta_2 - c_2\dot{\Theta}_2^2 \sin\Theta_2)\sin\Theta_2 - g\sin\Theta_2 \\ (-l_1\ddot{\Theta}_1 \sin\Theta_1 - l_1\dot{\Theta}_1^2 \cos\Theta_1 - l_2\ddot{\Theta}_2 \sin\Theta_2 - l_2\dot{\Theta}_2^2 \cos\Theta_2 - c_3\ddot{\Theta}_3 \sin\Theta_3 - c_3\dot{\Theta}_3^2 \cos\Theta_3)\sin\Theta_3 - g\cos\Theta_3 \\ -(l_1\ddot{\Theta}_1 \cos\Theta_1 - l_1\dot{\Theta}_1^2 \sin\Theta_1 + l_2\ddot{\Theta}_2 \cos\Theta_2 - l_2\dot{\Theta}_2^2 \sin\Theta_2 + c_3\ddot{\Theta}_3 \cos\Theta_3 - c_3\dot{\Theta}_3^2 \sin\Theta_3)\sin\Theta_3 - g\sin\Theta_3 \\ M_2 + K_{11}\ddot{\Theta}_1 + K_{12}\ddot{\Theta}_2 \cos(\Theta_1 - \Theta_2) + K_{13}\ddot{\Theta}_3 \cos(\Theta_1 - \Theta_3) + K_{14}\dot{\Theta}_2^2 \sin(\Theta_1 - \Theta_2) + K_{15}\dot{\Theta}_3^2 \sin(\Theta_1 - \Theta_3) + K_{16}\cos\Theta_1 \\ M_3 + K_{22}\ddot{\Theta}_2 + K_{21}\ddot{\Theta}_1 \cos(\Theta_1 - \Theta_2) + K_{23}\ddot{\Theta}_3 \cos(\Theta_2 - \Theta_3) - K_{24}\dot{\Theta}_1^2 \sin(\Theta_1 - \Theta_2) + K_{25}\dot{\Theta}_3^2 \sin(\Theta_2 - \Theta_3) + K_{26}\cos\Theta_2 \\ K_{33}\ddot{\Theta}_3 + K_{31}\ddot{\Theta}_1 \cos(\Theta_1 - \Theta_3) + K_{32}\ddot{\Theta}_2 \cos(\Theta_2 - \Theta_3) - K_{34}\dot{\Theta}_1^2 \sin(\Theta_1 - \Theta_3) - K_{35}\dot{\Theta}_2^2 \sin(\Theta_2 - \Theta_3) + K_{36}\cos\Theta_3 \end{bmatrix} \quad (9)$$

$$\begin{bmatrix} \dot{\Theta}_1 \\ \ddot{\Theta}_1 \\ \dddot{\Theta}_1 \\ \dot{\Theta}_2 \\ \ddot{\Theta}_2 \\ \dddot{\Theta}_2 \\ \dot{\Theta}_3 \\ \ddot{\Theta}_3 \\ \dddot{\Theta}_3 \end{bmatrix} = \begin{bmatrix} 0 & 1 & 0 & 0 & 0 & 0 & 0 & 0 & 0 \\ 0 & 0 & 1 & 0 & 0 & 0 & 0 & 0 & 0 \\ 0 & 0 & 0 & 0 & 0 & 0 & 0 & 0 & 0 \\ 0 & 0 & 0 & 0 & 1 & 0 & 0 & 0 & 0 \\ 0 & 0 & 0 & 0 & 0 & 1 & 0 & 0 & 0 \\ 0 & 0 & 0 & 0 & 0 & 0 & 0 & 0 & 0 \\ 0 & 0 & 0 & 0 & 0 & 0 & 0 & 1 & 0 \\ 0 & 0 & 0 & 0 & 0 & 0 & 0 & 0 & 1 \\ 0 & 0 & 0 & 0 & 0 & 0 & 0 & 0 & 0 \end{bmatrix} \cdot \begin{bmatrix} \Theta_1 \\ \dot{\Theta}_1 \\ \ddot{\Theta}_1 \\ \Theta_2 \\ \dot{\Theta}_2 \\ \ddot{\Theta}_2 \\ \Theta_3 \\ \dot{\Theta}_3 \\ \ddot{\Theta}_3 \end{bmatrix} \quad (8)$$

In (9) the parameters are defined as follows:

$$K_{11} = m_1 c_1^{\,2} + m_2 l_1^{\,2} + m_3 l_1^{\,2} + I_{x1}$$
$$K_{12} = K_{14} = K_{21} = K_{24} = m_2 l_1 c_2 + m_3 l_1 l_2$$
$$K_{13} = K_{15} = m_3 l_1 c_3$$
$$K_{16} = g(m_1 c_1 + m_2 l_1 + m_3 l_1)$$

$$K_{22} = m_2 c_2^{\,2} + m_3 l_2^{\,2} + I_{x2}$$
$$K_{23} = K_{25} = K_{32} = K_{35} = m_3 l_2 c_3$$
$$K_{26} = g(m_2 c_2 + m_3 l_2)$$

$$K_{31} = K_{34} = m_3 l_1 c_3$$
$$K_{33} = m_3 c_3^{\,2} + I_{x3}$$
$$K_{36} = m_3 g c_3$$

The EKF algorithm was implemented according to [10] as show below:

Measurement update is

$$\mathbf{K}_k = \mathbf{P}_k^{-}\mathbf{H}_k^{\,T}(\mathbf{H}_k\mathbf{P}_k^{-}\mathbf{H}_k^{\,T} + \mathbf{R}_k)^{-1} \quad (10)$$

$$\hat{\mathbf{x}}_k = \hat{\mathbf{x}}_k^{\,-} + \mathbf{K}(\mathbf{z}_k - \mathbf{h}(\hat{\mathbf{x}}_k^{\,-}, 0)) \quad (11)$$

$$\mathbf{P}_k = (\mathbf{I} - \mathbf{K}_k\mathbf{H}_k)\mathbf{P}_k^{-} \quad (12)$$

and time update is

$$\mathbf{P}_{k+1}^{-} = \mathbf{A}_k\mathbf{P}_k\mathbf{A}_k^{\,T} + \mathbf{Q}_k \quad (13)$$

The EKF initial state was set to actual system state at the initial time instance.

## 3 Results

The proposed method was verified on sit-to-stand transition of human subject. The results were compared to the reference measurements acquired by the Optotrak optical motion capture system. Measurement setup can be seen in Figure 4. Infrared markers were attached to subject's skin at key anatomical points denoting human joints. The marker motion trajectories were measured by Optotrak infrared cameras at sampling rate of 50Hz. Subject was standing on AMTI force plate which measured floor reaction forces needed. Optionally, the force plate can in ambulatory settings be substituted by shoe insole with force sensors. For assessing the seat contact in our experimental setup the multidimensional force sensor (JR3 Inc.) was used. However, in ambulatory setting a simple on/off switch would be sufficient for seat contact detection. Optical motion capture system was used to measure positional coordinates of markers with respect to reference coordinate frame. Numerical differentiation was accomplished for derivation of

velocities and accelerations. This procedure introduced numerical error to the input signals.

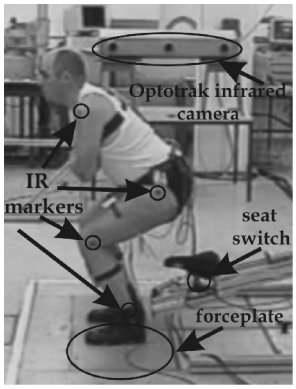


Fig. 4 – Measurement setup

For determining the moments $M_1$, $M_2$ and $M_3$ that act in the human joints and can not be directly measured by sensors, the inverse Newton-Euler approach was utilized. Overview of the algorithm used iteratively can be seen in Figure 5.

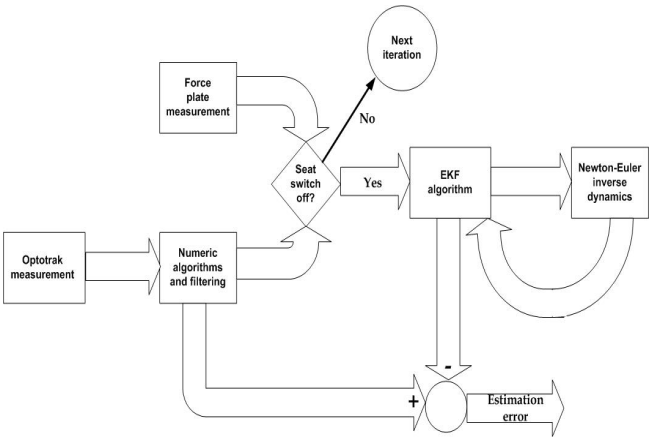


Fig. 5 – Block scheme of joint moment assessment

The obtained results of joint angle assessment compared to the reference measurements are presented in Figure 6. Figure 7 presents the angle estimation error, while Figure 8 depicts associated root mean square error (RMSE) values for each of angle estimate. From the results it is evident that proposed method shows good performance. The estimation error is smallest for shank angle with RMSE value of 1.582°, while the error is somewhat larger for thigh and HAT angles with RMSE values of 2.101° and 2.138°, respectively.

Some oscillations can be observed in $\Theta_2$ and $\Theta_3$ angle estimation. The oscillations are attributed to the fact that irregular oscillations happen near the angle of 90° where some components in Newton-Euler equations for joint moment calculation change sign, due to change in relative position of the segment and joint forces.

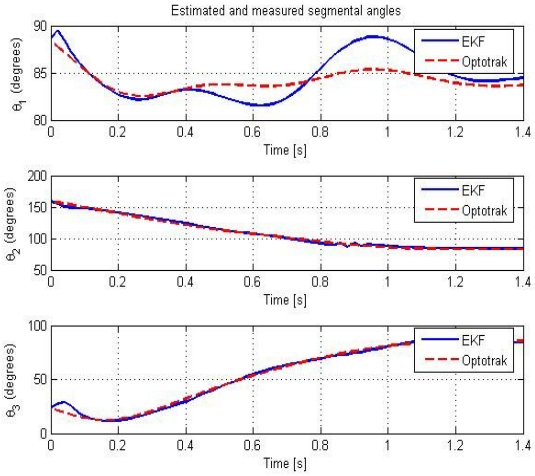


Fig. 6 – Comparison of reference measurements and estimation

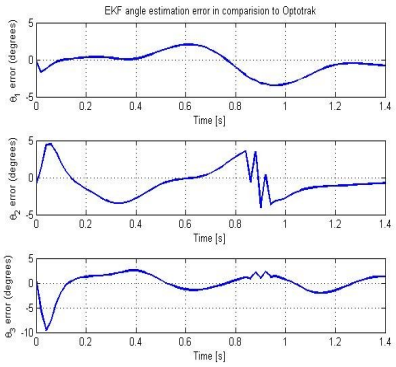


Fig. 7 – Estimation error

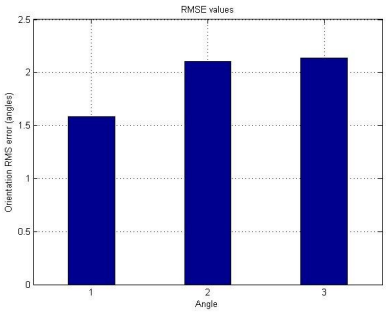


Fig. 8 – RMSE values

Comparison of moments calculated off-line using Optotrak data and moments calculated by iterative algorithm in EKF reveals good matching as presented in Figure 9 for the knee moment. The solid line in Figure 9 corresponds to the knee moment calculated inside EKF loop from EKF estimates, while the dotted line represents knee moment calculated off-line from data measured with Optotrak.

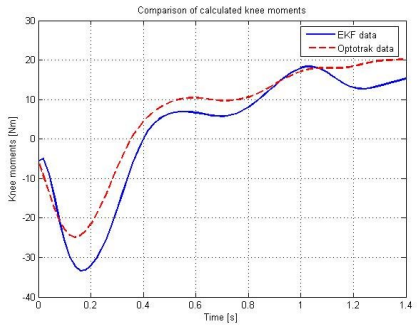


Fig. 9 – Comparison of assessed knee moments during sit-to-stand transfer

## 4 Conclusion

The model based inertial sensing method for estimation of human body motion kinematics based on body model and Extended Kalman filtering is developed.

In motion equations the joint friction was omitted for simplicity and computational efficiency and restriction of the motion to the sagittal plane was introduced. We believe higher level of accuracy could be achieved by inclusion of some additional phenomena's or by making model assumptions less restrictive. The EKF structure was designed with objective of computational simplicity and efficiency in mind.

Obtained results show good tracking capability for all three estimated segmental angles. The best tracking is achieved for the shank (RMSE: $1.582^0$), although other angles estimates also have low RMSE values ($2.101^0$ and $2.138^0$, respectively). This can be explained by the fact that equations describing the shank motion have simpler form in respect to others and also range of motion is smaller than that of the other segments. Small oscillations are present in thigh and HAT segment estimation at time of 0.9 s after start. The oscillations are attributed to Newton-Euler inverse dynamic equations for knee and hip joint which change their form due to the change in sign for some of its components and can be reduced with fine-tuning of EKF parameters. EKF parameters were manually tuned during filter design.

The presented approach and its results are the first stage in development phase of low cost inertial sensor based kinematic measurement system. For further improvements some modifications in the method structure and measurement procedure are planned. Optimization of EKF filter tuning (selection of matrices **R**, **Q** and **P**) is planned based on tuning criteria [12]. Higher sampling rate should also improve accuracy of estimation. Finally the extensive testing is planned based on data acquired by inertial sensors in sit-to-stand motion of a group of healthy and impaired subjects.

*References:*

[1] R. Bogue, MEMS sensors: past, present and future, *Sensor Review,* Vol. 27, No. 1, 2007, pp. 7-13

[2] X. Yun, E. R. Bachmann, Design, implementation, and experimental results of a quaternion-based kalman filter for human body motion tracking, *IEEE transactions on Robotics*, Vol. 22, No. 6, 2006, pp. 1216-1227

[3] R. Moe-Nilssen, A new method for evaluating motor control in gait under real-life environmental conditions. Part 1: The instrument, *Clinical Biomechanics*, Vol. 13, 1998, pp. 320-327

[4] R, Kamink, J. Musić, H. Burger, M. Munih, T. Bajd, Design of inertial motion sensors and its usage in biomechanical analysis, *In. proc. of EPE'06*, 2006, 511-516

[5] M. C. Boonstra et. al. , The accuracy of measuring the kinematics of rising from a chair with accelerometers and gyroscopes, *Journal of Biomechanics*, Vol. 39, 2006, pp. 354-358

[6] D. Giansanti, V. Macellari, G. Maccioni, A. Cappozzo, Is it feasible to reconstruct body segment 3-D position and orientation using accelerometer data?, *IEEE Transactions on Biomedical Engineering*, Vol. 50, No. 4, 2003, pp. 476-483

[7] D. Roetenberg, P. J. Slycke, P. H. Veltink, Ambulatory position and orientation tracking fusing magnetic and inertial sensing, *IEEE Transactions on Biomedical Engineering*, Vol. 54, No. 5, 2007, pp. 883-890

[8] J. Musić, R. Kamnik, M. Munih, Model based inertial sensing of human body motion kinematics in sit-to-stand movement, *In. proc. of Eurosim'07*, 2007

[9] H. Hemami, V. C. Jaswa, On the three-link model of the dynamics of standing up and sitting down, *IEEE Transactions on Systems, Man, and Cybernetics*, Vo. SMC-8, No. 2, 1978, pp. 115-120

[10] R. Kamnik, F. Boettiger, K. Hunt, Roll dynamics and lateral load transfer estimation in articulated heavy freight vehicles, *Journal of Automobile Engineering,* Vol. 217, Part D, 2003, pp. 985-997

[11] P.D. Leva, Adjustment to Zatsiorksy-Seluyanov's segment inertia parameters, *Journal of Biomechanics,* Vol. 29, No. 9, 1996, pp. 1223-1230

[12] P. Abbel, A. Coates, M. Montermerlo, A. Y. Ng, S. Thrun, Discriminative training of Kalman filters, *In proc. of Robotics: Science and Systems*, 2005